Volume 53, issue 2, February 2011 ISSN 0010-938X

ELSEVIER

CORROSION SCIENCE

The Journal on Environmental Degradation of Materials and its Control

Editor-in-Chief: G. T. BURSTEIN, University of Cambridge, U.K.

An Official Journal of the Institute of Corrosion

CONTENTS

Contents continued on outside back cover

http://www.elsevier.com/locate/corsci

Corrosion Science 53 (2011) 645–654

Contents lists available at ScienceDirect

Corrosion Science

journal homepage: www.elsevier.com/locate/corsci

Corrosion behavior of commercially pure Mg and ZM21 Mg alloy in Ringer's solution – Long term evaluation by EIS

M. Jamesh, Satendra Kumar, T.S.N. Sankara Narayanan *

National Metallurgical Laboratory, Madras Centre CSIR Complex, Taramani, Chennai 600 113, India

ARTICLE INFO

Article history:
Received 24 May 2010
Accepted 17 October 2010
Available online 23 October 2010

Keywords:
A. Alloy
A. Magnesium
B. EIS
B. IR spectroscopy
C. Anodic dissolution

ABSTRACT

Evaluation of the corrosion behavior of commercially pure magnesium (CP-Mg) and ZM21 Mg alloy immersed in Ringer's solution for 92 h by electrochemical impedance spectroscopy (EIS) is addressed. The formation of a compact layer of well-developed rod-like aragonitic $CaCO_3$ crystals and its subsequent thickening with increase in immersion time offers a higher corrosion protective ability for ZM21 Mg alloy. The formation of a mud-crack pattern and a large number of clusters of needle-like crystals offers a relatively lower corrosion resistance for CP-Mg. The study suggests that ZM21 Mg alloy is a promising candidate material for the development of degradable implants.

1. Introduction

The development of biodegradable implants has become one of the interesting research topics among the biomaterial scientists [1–3]. The objective of achieving *in vivo* biodegradation of the implant with time without any undesirable effect to the human body is indeed fascinating. The biodegradable implant should stay in the human body only for the time it takes to fix the problem. Subsequently, it should be gradually dissolved, absorbed, consumed or excreted, without warranting a secondary surgery [4]. This approach considers corrosion as a desirable materials property, rather than a limitation. Biodegradable implants provide a viable option to solve the problems associated with permanent implants such as, restenosis, thrombosis, permanent physical irritation, and inability to adapt to growth and changes in human body [4]. Polymer based biodegradable implants such as those made of poly-L-lactic acid have been known for some time [5]. Recently, metallic-based biodegradable implants are also emerging [6]. Polymer based biodegradable implants have an unsatisfactory mechanical strength, which limit their application whereas the metallic based ones is expected to provide a better solution in this respect.

In recent years, Mg and its alloys are considered for use as biodegradable implant materials for bone implants [7] as well as for cardiovascular stents [8–11]. The choice is made based on the fact that, Mg is not toxic to the human body and the dissolution of Mg is not likely to cause any adverse side effects. In fact, Mg is an essential element and found in large amounts in the human body. The presence of Mg in the bone system is also considered beneficial to bone strength and growth [12]. The specific density and Young's modulus of Mg are closer to bone than the commonly used metallic implant materials, which enables a decrease in stress at the bone/implant interface, stimulate bone growth and increase the implant stability [13]. Mg possesses greater fracture toughness over ceramic biomaterials, higher strength than biodegradable plastics, and favorable elastic modulus than commonly used metallic implant materials. Mg takes part in many metabolic reactions and biological mechanisms, including involvement in the formation of biological crystal apatite [14] (which is important for metallic bone implants). It is also a co-factor for many enzymes and stabilizes the structures of DNA and RNA [15]. Mg can be beneficial from a physiological standpoint, since magnesium deficiencies in the human body significantly contribute to cardiovascular disease [16]. Low serum Mg levels are associated with an increased risk for neurological events in patients having symptomatic peripheral artery disease [17]. In spite of the numerous advantages, the use of Mg as a biodegradable implant has been restricted because of some major limitations. Mg usually corrodes rapidly in body fluid, which leads to the generation of a large volume of hydrogen gas and a remarkable increase in local pH value of body fluid. Accumulation of the hydrogen bubbles in gas pockets adjacent to the implant would cause a delay in healing of the wound and lead to necrosis of tissues [18]. In the worst case, when the hydrogen bubbles are relatively large, there is an increased risk of blockage of the blood stream, causing death of a patient. The local alkalization can unfavorably affect the pH dependent physiological reaction balances in the vicinity of the Mg implant and may even lead to an alkaline poisoning effect if the local *in vivo* pH value exceeds 7.8 in that region [19].

* Corresponding author. Tel.: +91 44 2254 2077; fax: +91 44 2254 1027.
E-mail address: tsnsn@rediffmail.com (T.S.N. Sankara Narayanan).

0010-938X/$ - see front matter © 2010 Elsevier Ltd. All rights reserved.
doi:10.1016/j.corsci.2010.10.011

Alloying and surface treatment are the viable options to improve the corrosion resistance of Mg in body fluid. The improvement in corrosion resistance of Mg by alloying has been addressed by many researchers [20–27]. However, when the magnesium alloy is dissolved, the alloying elements will also be absorbed in the human body. Hence, alloying of Mg with elements such as Al, Zr, Pr, Ce, and Y is limited due to their toxicity [19,28–30]. Based on the *in vitro* corrosion rates of several magnesium alloys, Song [19] has pointed out that Ca, Mn and Zn could be the appropriate alloying elements. Alloying of Ca leads to Mg_2Ca precipitation, which would induce the formation of a galvanic cell, resulting in acceleration of the rate of corrosion and hydrogen evolution [31]. Zn and Mn can be tolerated in the human body. Zn is an essential element in the human body and it provides strength for magnesium alloys due to solid solution strengthening [1,32]. Similar to zinc, Mn is also essential to the human body. Mn helps to refine the grain size, enhance the ductility and improve the tensile strength of Mg alloys [1,33]. Small additions of Mn have been shown to increase the corrosion resistance of the Mg alloy, which also helps to reduce the effects of metallic impurities [34,35]. As a result, studies on Mg alloys having Mn and Zn as alloying elements assumes significance. Xu et al. [36] have studied the

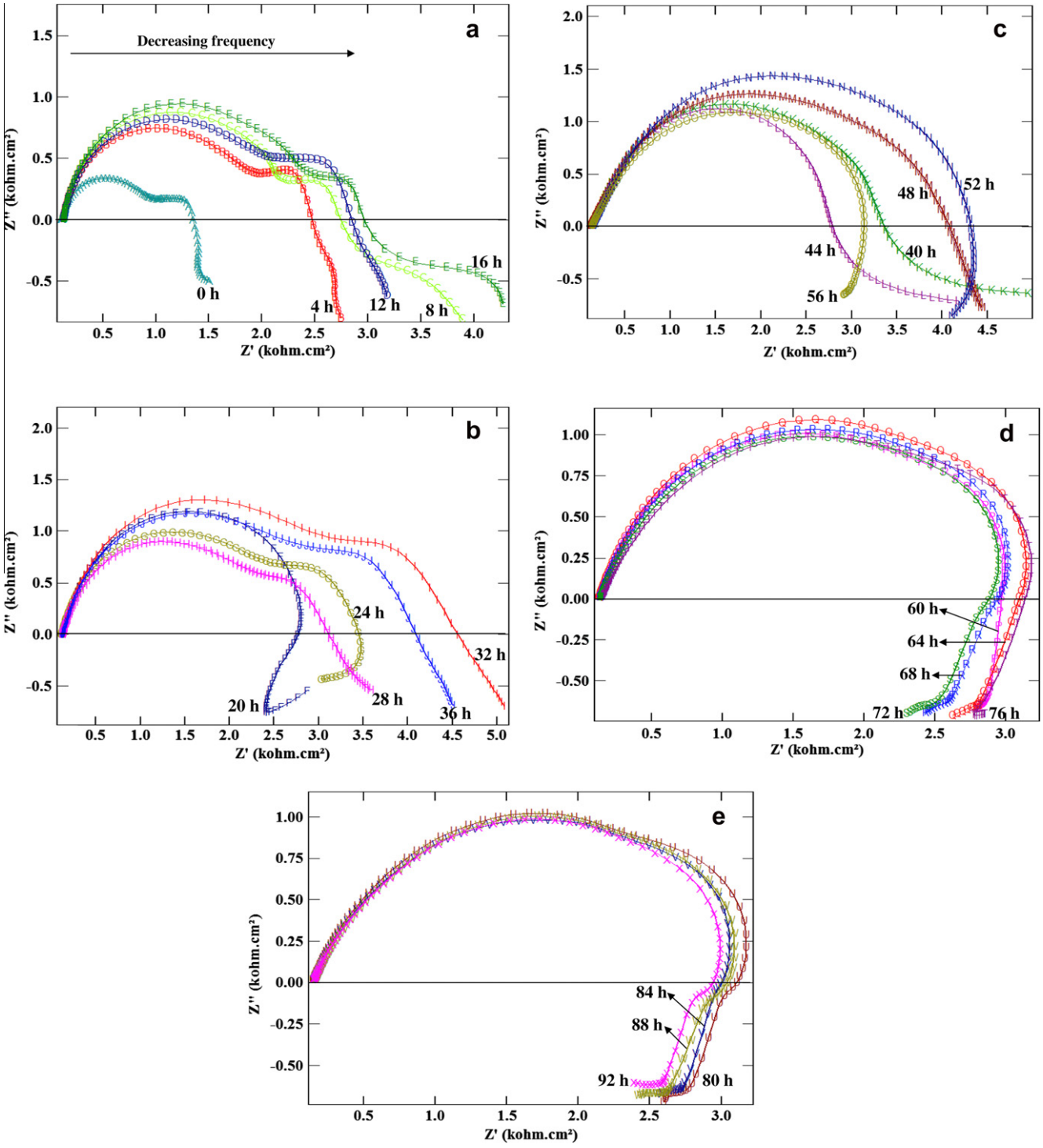

Fig. 1. Nyquist plots of CP-Mg in Ringer's solution recorded at every 4 h interval at their respective open circuit potentials for 92 h.

in vivo corrosion behavior of Mg–Mn–Zn alloy for bone implant application. The microstructure, mechanical properties, corrosion resistance and biocompatibility of Mg–Zn–Mn alloys for biomedical application was studied by Zhang et al. [37]. A recent study on the biocompatibility of resorbable Mg–Zn alloy reveals that this alloy has no effect on the chromaticness, structure or function of heart, liver, kidney, or spleen [38]. The bio-corrosion behavior of Mg–Zn–Mn alloy for biomedical applications was studied recently by Rosalbino et al. [39].

The corrosion behavior of bare, alloyed and surface modified Mg and its alloys in simulated body fluids was evaluated by monitoring the extent of hydrogen evolution, potentiodynamic polarization and electrochemical impedance spectroscopy (EIS) studies [1–4,7,9,19]. The extent of hydrogen evolution is a quantitative indicator of the rate of corrosion of Mg and its alloys in the simulated body fluid. Potentiodynamic polarization and EIS studies are also useful to estimate the rate of corrosion and to rank the corrosion protective ability of Mg and its alloys. However, the formation of corrosion products on the surface of Mg and its alloys modifies the rate of corrosion. Hence, it is essential to monitor the long-term corrosion behavior to estimate the longevity of Mg-based implants in the human body. EIS is essentially a steady state technique that is capable of accessing relaxation phenomena whose relaxation times vary over orders of magnitudes and permits single averaging within

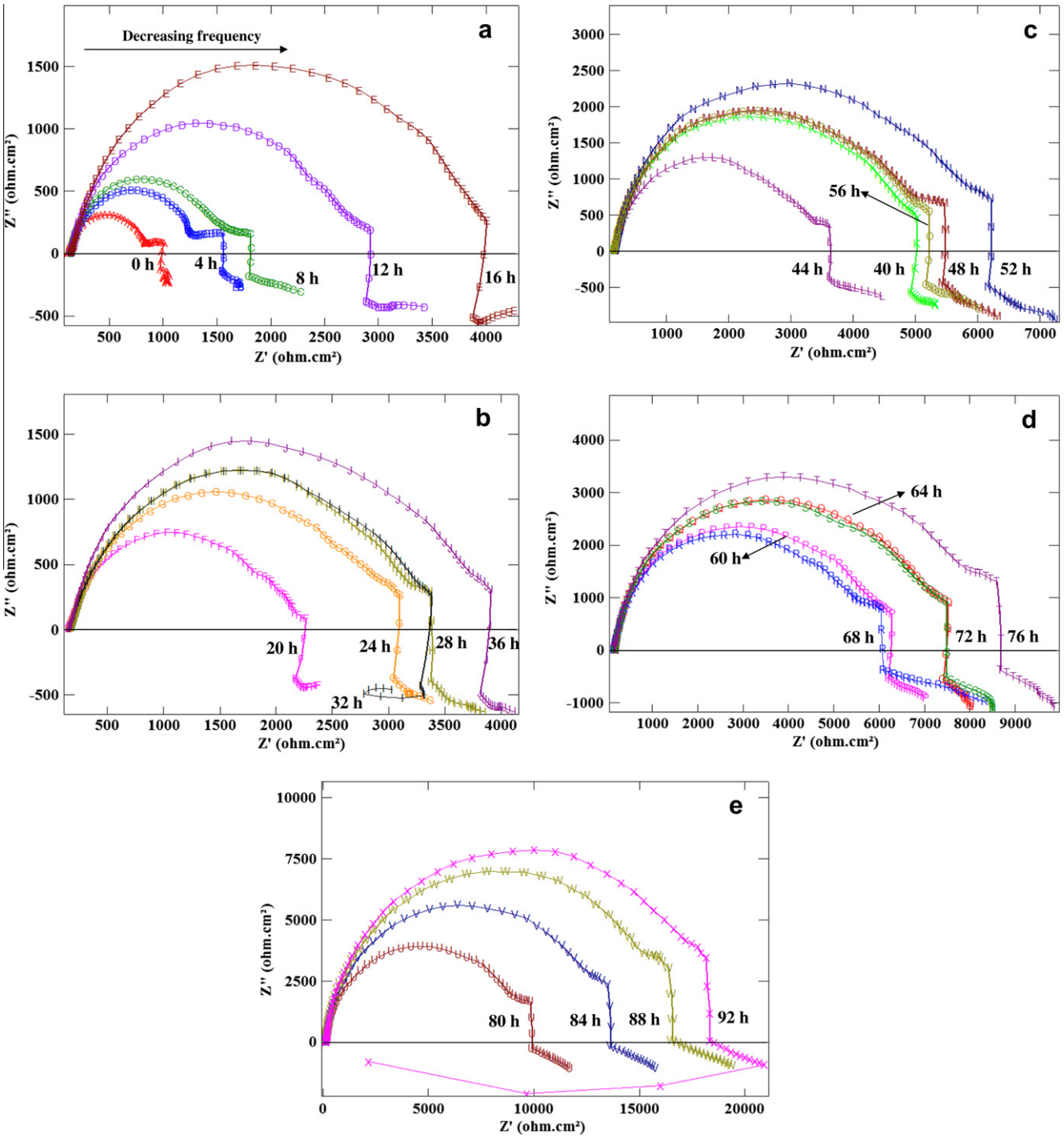

Fig. 2. Nyquist plots of ZM21 Mg alloy in Ringer's solution recorded at every 4 h interval at their respective open circuit potentials for 92 h.

a single experiment to obtain high precision levels. EIS is an ideal method to monitor the long-tem corrosion behavior. In this perspective, the present study evaluates the corrosion behavior of commercially pure magnesium (CP-Mg) and ZM21 Mg alloy in simulated body fluid by EIS for 92 h.

2. Experimental details

CP-Mg (composition in wt.%: Zn: 0.01; Mn: 0.008; Cu: 0.004; Fe: 0.05; Ni: 0.001; Pb: 0.01; Sb: 0.06; Al: 0.02; and Mg: Balance) and ZM21 Mg alloy (composition in wt.%: Zn: 2.03; Mn: 0.81; and Mg: Balance) were used as the substrate materials in this study. Ringer's solution has already been used to evaluate the corrosion behavior of metallic implant materials [40–47]. Ringer's solution, having a chemical composition [39,42–47] (in mM) of 154 NaCl, 2.2 $CaCl_2$, 5.8 KCl and 2.4 $NaHCO_3$ (pH: 7.8) was used as the electrolyte solution. All the experiments were performed at 37 ± 1 °C. The corrosion behavior of CP-Mg and ZM21 Mg alloy was evaluated by electrochemical impedance spectroscopic (EIS) and potentiodynamic polarization studies using a potentiostat/galvanostat/frequency response analyzer of ACM instruments (model: Gill AC). The details of the EIS and potentiodynamic polarization experiments were reported in our earlier papers [42–44]. Before performing the corrosion studies, the CP-Mg and ZM21 Mg alloy samples were abraded with various grades of SiC paper followed by mechanically polishing with 0.3 μm alumina paste to a mirror finish, rinsed with deionized water and dried using a stream of compressed air. The cleaned CP-Mg and ZM21 Mg alloy samples formed the working electrode while a saturated calomel electrode (SCE) and a graphite rod served as the reference and auxiliary electrodes, respectively. These electrodes were placed in a flat cell in such a way that only 1 cm^2 area of the working electrode was exposed to the Ringer's solution. The EIS study of CP-Mg and ZM21 Mg alloy samples was conducted at their respective OCPs. The measurements were carried out at every 4 h interval for 92 h. The impedance spectra were recorded using an excitation voltage of 32 mV rms (root mean square) in the frequency range between 10 kHz and 0.01 Hz. Based on the nature of the Nyquist plots, an equivalent electrical circuit was proposed to account for the corrosion behavior. The electrochemical parameters were obtained after fitting the data using the proposed model. Bode impedance and phase angle plots were also recorded for analysis of the corrosion performance. Potentiodynamic polarization measurements of CP-Mg and ZM21 Mg alloy samples were carried out immediately after immersion (0 h) and after immersion in Ringer's solution for 48 h. The potential of CP-Mg/ZM21 Mg alloy samples was scanned from −250 mV in the cathodic direction to +250 mV in the anodic direction from the respective open circuit potential (OCP) vs. SCE at a scan rate of 100 mV/min. The corrosion potential (E_{corr}) and corrosion current density (i_{corr}) were determined from the polarization curves by Tafel extrapolation method. The EIS and potentiodynamic polarization studies were repeated at least three times to ensure reproducibility of the test results. The morphological feature and chemical nature of the corrosion product formed on CP-Mg and ZM21 Mg alloy after 92 h of immersion in Ringer's solution were assessed by scanning electron microscope (SEM) and energy dispersive X-ray analysis (EDX). FT-IR spectroscopy is also used to identify the chemical nature of the corrosion products.

3. Results and discussion

The Nyquist plots of CP-Mg and ZM21 Mg alloy in Ringer's solution recorded at every 4 h interval for 92 h are shown in Figs. 1 and 2, respectively. The choice of such a long duration is essential to estimate the longevity of these materials for implant application since the rate of corrosion of CP-Mg and ZM21 Mg alloy in Ringer's solution will be modified by the corrosion products formed on their surface. The terminology of "long term" is generally used for studies performed for a longer period, in years. In the present study, this terminology is used to distinguish it from the regular electrochemical corrosion studies that are performed within an hour or two. The EIS spectra of CP-Mg and ZM21 Mg alloy are characterized by three well-defined loops: a capacitive loop in the high frequency region, a capacitive loop in the medium frequency region and an inductive loop in the low frequency region, suggesting the involvement of three time constants. The capacitive loop observed at the high frequency region is attributed to the charge transfer reaction in the electric double layer formed at the interface between the metal surface and the corrosive medium [48]. The capacitive loop observed at the middle frequency region is related to the mass transport in solid phase, i.e., to the diffusion of ions through the corrosion product layer [49]. The inductive loop observed at the low frequency region is related to the adsorption processes [50]. The transition from the capacitive to the inductive behavior has caused a change in shape of the curves below 0.8 Hz. There are no changes in the pattern/trend between triplicate measurements and the reproducibility of test results is verified. To analyze the EIS spectra of CP-Mg and ZM21 Mg alloy, an equivalent electrical circuit model shown in Fig. 3 is used. In this model, R_s represents the solution resistance, R_{ct} is the charge transfer resistance, i.e., the resistance to the electron transfer of the faradic process on CP-Mg/ZM21 Mg alloy, in parallel to the double layer capacitance, C_{dl}. Since the Nyquist plots of CP-Mg and ZM21 Mg alloy exhibit depressed semicircles, a constant phase element, CPE_1 is used instead of C_{dl} in the proposed model. An additional constant phase element, CPE_2 and a resistance, R_f were also introduced in to the model to account for the capacitance and resistance of the corrosion product layer formed on the surface of CP-Mg/ZM21 Mg alloy. To account for the inductive behavior, an inductor, L and a resistance, R_L were introduced in this model. Xin et al. [51,52] and Song et al. [53] have also used a similar model to explain the corrosion behavior of AZ31 Mg alloy and, ZrO_2/Zr and ZrN/Zr coated AZ91 Mg alloy in simulated body fluids. The validity of the model is confirmed based on the better non-linear least square fitting of the experimental data within 5% error. The

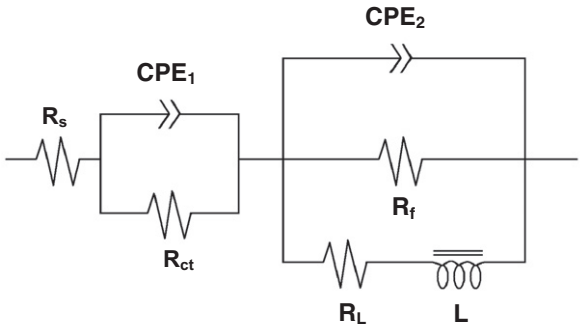

Where

R_s	: Electrolyte resistance
R_{ct}	: Charge transfer resistance
CPE_1	: Constant phase element related to the double layer capacity
R_f	: Surface film resistance
CPE_2	: Constant phase element related to film capacity
L	: Induction related to adsorbed intermediates during the corrosion of CP-Mg/ZM 21 Mg alloy
R_L	: Inductive resistance

Fig. 3. Equivalent electrical circuit used to analyze the EIS data recorded during corrosion of CP-Mg and ZM21 Mg alloy in Ringer's solution for 92 h.

transition from the capacitive to the inductive behavior observed below 0.8 Hz did not cause any error in fitting. The fitting obtained for the EIS data of CP-Mg (24 h immersion) and ZM21 Mg alloy (32 h immersion) are shown in Fig. 4.

The variation in R_{ct} and CPE_1 of CP-Mg and ZM21 Mg alloy as a function of time, are plotted in Fig. 5a and b, respectively. For CP-Mg, an increase in R_{ct} and a slight decrease in CPE_1 are observed up to 12 h. This is due to the formation of insoluble corrosion products on the surface of CP-Mg, which hinders the charge transfer process. Between 12 and 60 h of immersion, some fluctuations in R_{ct} and CPE_1 are observed, which indicates a simultaneous occurrence of dissolution of Mg through the pores or defects and formation of the corrosion product layer following the increase in interfacial pH. The near saturation in R_{ct} and CPE_1 observed between 60 and 92 h suggest coverage of the surface of CP-Mg with the corrosion products. For ZM21 Mg alloy, a steady increase in R_{ct} and a decrease in CPE_1 are observed up to 16 h. Between 16 and 68 h of immersion, some fluctuations in R_{ct} and CPE_1 are observed. As explained earlier, formation of insoluble corrosion products and, simultaneous dissolution of the Mg alloy and formation of the corrosion product layer are considered responsible for these observations. Unlike CP-Mg, a sudden increase in R_{ct} and a decrease in CPE_1 are observed between 68 and 92 h for ZM21 Mg alloy. This could be due to the thickening of the corrosion product layer,

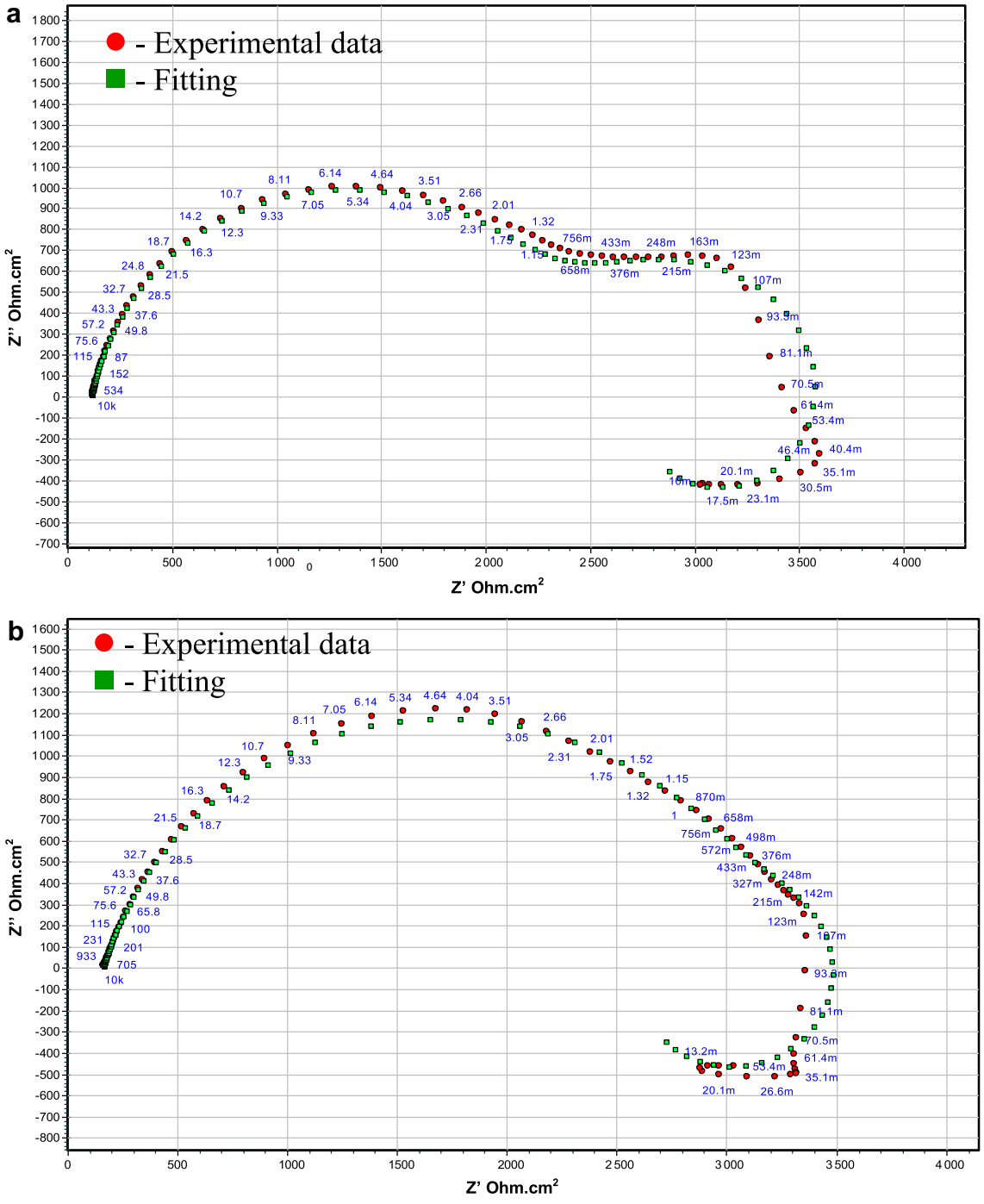

Fig. 4. Non-linear least square fitting obtained for the EIS data of CP-Mg and ZM21 Mg alloy (a) CP-Mg (24 h immersion); (b) ZM21 Mg alloy (32 h immersion).

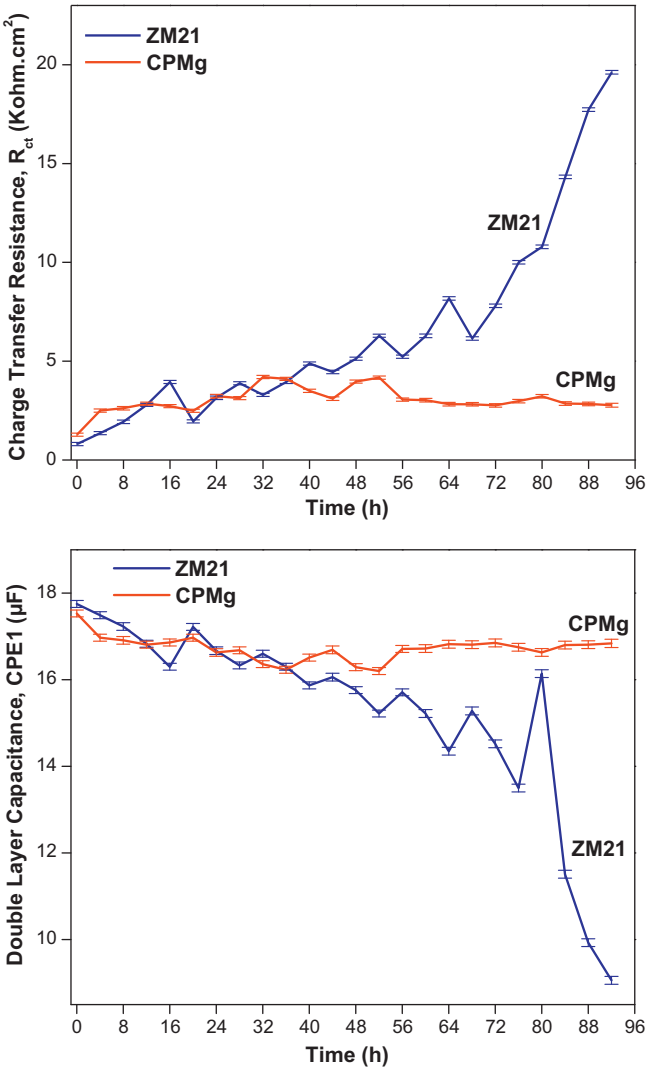

Fig. 5. Variation in charge transfer resistance, R_{ct} (a) and double layer capacity, CPE1 (b) of CP-Mg and ZM21 Mg alloy in Ringer's solution recorded as a function of time.

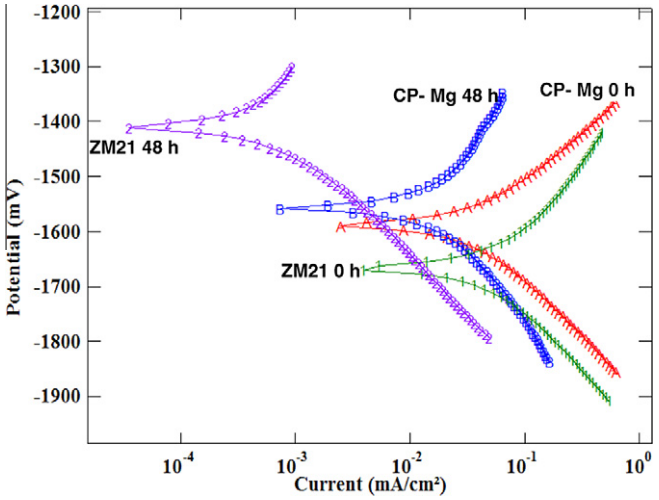

Fig. 6. Potentiodynamic polarization curves of CP-Mg and ZM21 Mg alloy in Ringer's solution recorded immediately (0 h) and after 48 h of immersion.

which acts as an effective barrier for the charge transfer process. Anderson and Stumpf [54] and Lunder et al. [55] have reported that the surface film covering Mn-containing magnesium alloys contains an appreciable fraction of manganese oxides/hydroxides, which helps to enhance the surface passivity. According to them, incorporation of oxidized manganese in the brucite layered structure, via substitution of the magnesium cations, hinder incorporation of chloride anions in the $Mg(OH)_2$ lattice, thus enhancing the protective performance of the surface film. This view is further confirmed recently by Rosalbino et al. [39]. The improved corrosion resistance of ZM21 Mg alloy compared to CP-Mg could also be due to the incorporation of oxidized manganese in the brucite-layered structure.

In order to confirm the corrosion behavior exhibited by CP-Mg and ZM21 Mg alloy in EIS studies, potentiodynamic polarization curves are recorded immediately (0 h) and after 48 h of immersion in Ringer's solution (Fig. 6). A shift in E_{corr} towards noble direction and a decrease in i_{corr} are observed with increase in immersion time from 0 to 48 h for both CP-Ti and ZM21 Mg alloy; among them the effect is well pronounced for ZM21 Mg alloy. The extent of nobler shift in E_{corr} (from −1669 to −1411 mV vs. SCE) and decrease in i_{corr} (from 41.70 to 0.19 μA/cm^2) is relatively high for ZM21 Mg alloy when compared to that of CP-Mg (from −1589 to −1558 mV vs. SEC; and from 23.05 to 7.50 μA/cm^2). The inference from polarization studies support the results obtained from EIS studies.

The morphological features of CP-Mg and ZM21 Mg alloy after immersion in Ringer's solution for 92 h are shown in Fig. 7a and b, respectively. The formation of mud-crack patterns (marked by circles in Fig. 7a) and large number of clusters of needle-like crystals are evident on the surface of CP-Mg. In contrast, no mud-crack pattern could be observed on the surface of ZM21 Mg alloy, which is covered with a compact layer of well-developed rod-like crystals. The EDX analysis performed on selective regions (marked by white rectangles in Fig. 7a and b) indicates that the corrosion products formed on the surface of CP-Mg and ZM21 Mg alloy are rich in O, C, Ca and Mg. The elemental analysis suggests that the corrosion product could be a mixture of $CaCO_3$ and $Mg(OH)_2$, with $CaCO_3$ as the predominant species.

Among the allotropic forms of $CaCO_3$, calcite is thermodynamically more stable than aragonite and vaterite. The solubility product K_{sp} of calcite (3.36×10^{-9}) is slightly lower than aragonite (4.6×10^{-9}) and about an order lower than vaterite (1.2×10^{-8}) [56]. Hence, the calcite form of $CaCO_3$ is expected to be the predominant species. However, earlier studies have shown that presence of sufficient concentration of Mg^{2+} ion would promote the aragonite form of $CaCO_3$ [57–63]. According to Reddy and Nancollas [64], precipitation of aragonitic $CaCO_3$ could occur at temperatures as low as 25 °C. Tai and Chen [62] have reported that at a fixed temperature of 24 °C, aragonitic $CaCO_3$ particles are the predominant product (~90% of total polymorphs, ~10% calcite) when solution pH is roughly 11. In the present study, corrosion of CP-Mg and ZM21 Mg alloy would enable sufficient concentration of Mg^{2+} ions at the metal-solution interface. In order to get an insight about the pH of the electrolyte, the change in pH of the Ringer's solution following immersion of CP-Mg and ZM21 Mg alloy is measured for the entire duration of 92 h. For CP-Mg, the pH is increased from 7.80 to 8.36 whereas for ZM21 Mg alloy, the pH is increased from 7.80 to 8.09, after 92 h of immersion (Fig. 8). During the first 10 h of immersion, the extent of increase in pH is high. A moderate increase in pH is observed between 10 and 30 h while saturation in pH is reached beyond 30 h of immersion (Fig. 8). However, this change is pH represents the bulk while the interfacial pH would be much higher than that is measured at the bulk of the solution. The attack of the chloride ions on $Mg(OH)_2$ would lead to an increase in interfacial pH > 10. Hence, the $CaCO_3$ precipitate formed on the surface of CP-Mg and ZM21 Mg alloy could be the aragonite

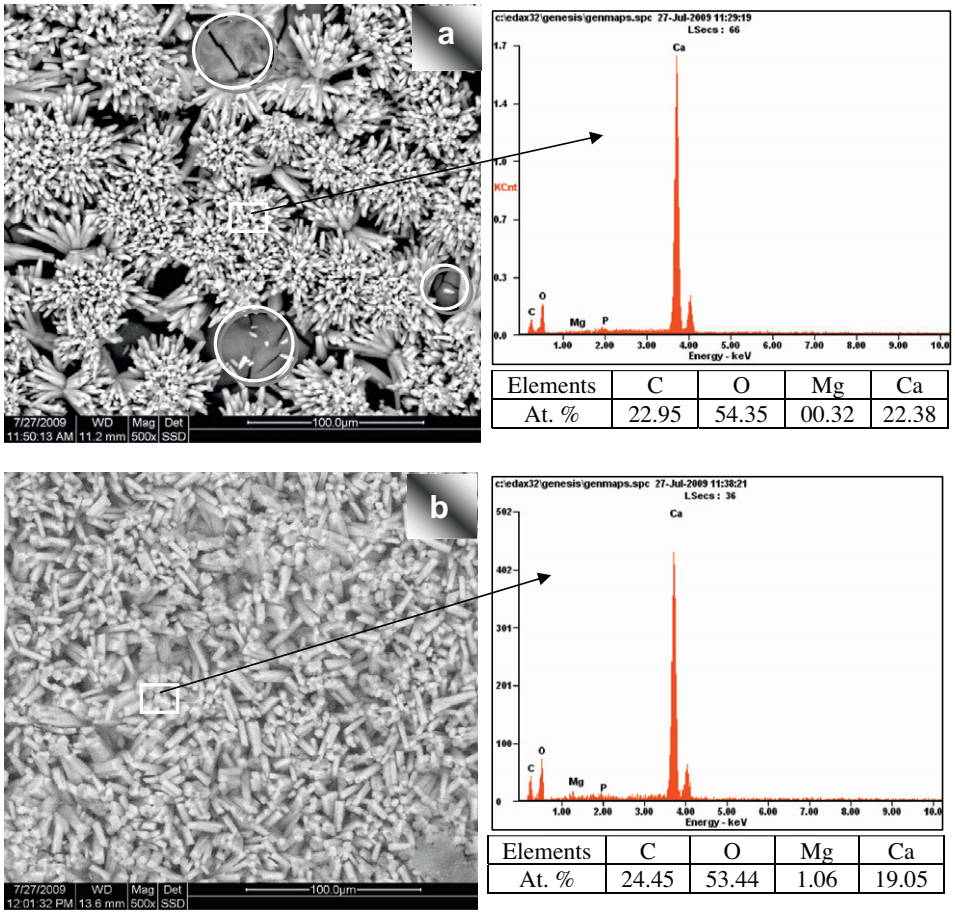

Fig. 7. Morphological features and chemical nature of the precipitate formed on CP-Mg (a) and ZM21 Mg alloy (b) after immersion in Ringer's solution for 92 h.

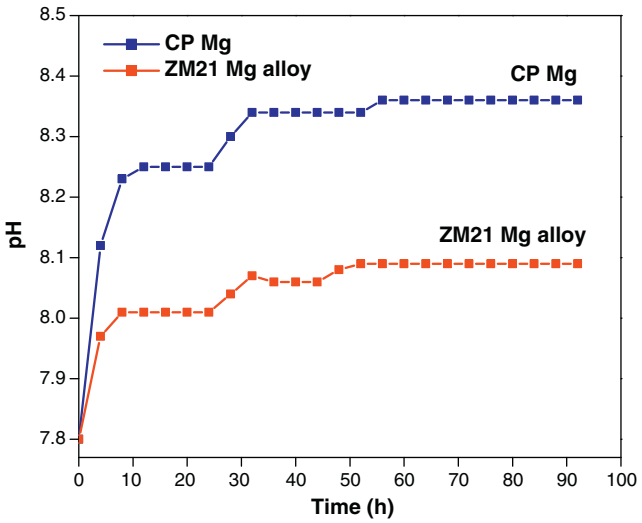

Fig. 8. Change in pH of the Ringer's solution during immersion of CP-Mg and ZM21 Mg alloy recorded during the entire duration of 92 h.

form. To confirm the nature of the $CaCO_3$ precipitate, the corrosion product layer formed on the surface of CP-Mg and ZM21 Mg alloy were carefully removed and subjected to FT-IR analysis. The FT-IR spectra of the corrosion products formed on CP-Mg and ZM21 Mg alloy are shown in Fig. 9a and b, respectively. It is evident that the nature of the corrosion products formed on the surface of CP-Mg and ZM21 Mg alloy are quite similar. The bands at 1082 cm^{-1} (moderate), 854/855 cm^{-1} (very strong), 712 cm^{-1} (strong), 699 cm^{-1} (moderate) can be assigned to the aragonite form of $CaCO_3$. The broad peak at 1478/1479 cm^{-1} and the peaks at 1788 and 2521 cm^{-1} can be assigned to the carbonate stretching modes of $CaCO_3$. The FTIR spectra further confirms that the corrosion product is the aragonite form of $CaCO_3$.

Yao et al. [65] have reported that the corrosion product formed on the surface of pure Mg in 3% NaCl solution was more hydrated than those formed in distilled water. The presence of a relatively higher concentration of chloride ions in the Ringer's solution used in the present study would lead to hydration of the corrosion product. The broad peak at 3436/3433 cm^{-1} (Fig. 9) confirms that the corrosion product layer is indeed hydrated. The hydration would lead to the conversion of cubic magnesium oxide to hexagonal magnesium hydroxide, with twice the increase in volume compared to the oxide, thus causing cracks in the layer [65,66]. Godard et al. [67] have suggested that $Mg(OH)_2$ (brucite) has a hexagonal crystal structure and easily undergoes basal cleavage, leading to cracking and curling of the corrosion product layer. Hence, the formation of mud-crack patterns (marked by circles in Fig. 7a) could be due to $Mg(OH)_2$. The peak observed at 3697 cm^{-1} (Fig. 9), which can be assigned to the O–H stretching mode also supports the view of formation of $Mg(OH)_2$.

Uan et al. [68] have correlated the morphological and microstructural characteristics and suggested that the growth of the aragonitic $CaCO_3$ layer on the surface of the Mg alloy occurs in two-stages. Lateral growth of the aragonitic $CaCO_3$ layer and formation of a thin continuous $CaCO_3$ film is the first stage while thickening of the $CaCO_3$ film is the second stage. A careful analysis of the morphological features of the corrosion product layer

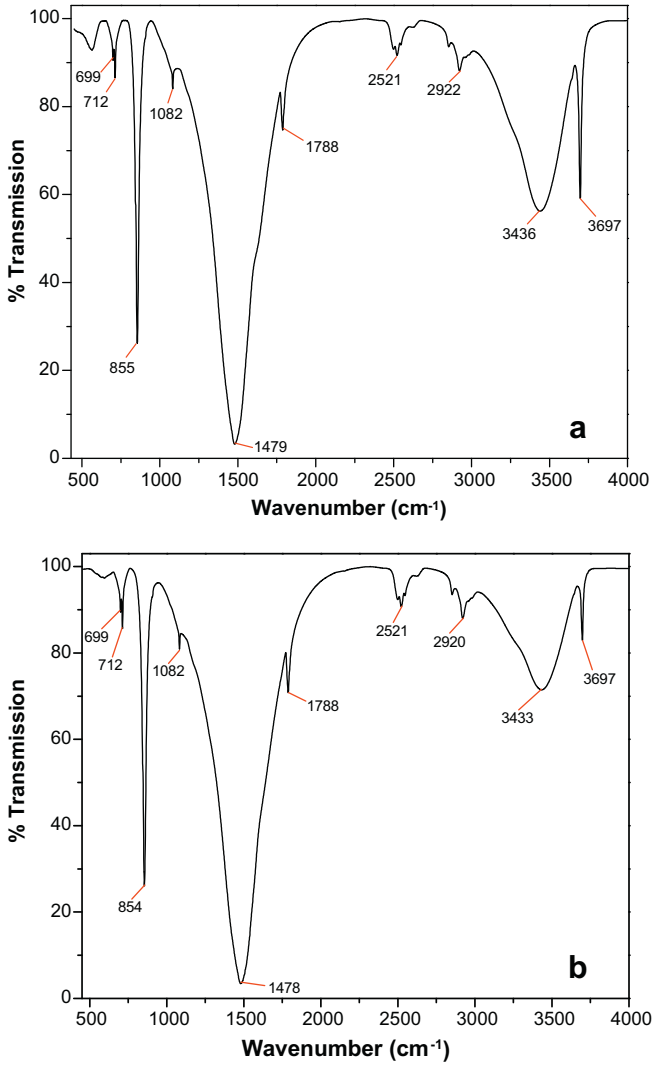

Fig. 9. FT-IR spectra of the corrosion products formed on (a) CP-Mg; and (b) ZM21 Mg alloy.

formed on CP-Mg and ZM21 Mg alloy reveals that both the first and second stage of growth of aragonitic $CaCO_3$ occurs on ZM21 Mg alloy whereas the second stage of growth is delayed for CP-Mg.

The change in electrochemical behavior as a function of immersion time assessed by EIS, the morphological features assessed by SEM and the nature of corrosion products assessed by EDX analysis and FT-IR spectroscopy, a pictorial model is proposed (Fig. 10) to explain the mechanism of corrosion of CP-Mg and ZM21 Mg alloy in Ringer's solution. This model schematically illustrates the various stages of the corrosion process of CP-Mg and ZM21 Mg alloy. When CP-Mg and ZM21 Mg alloy encounters the Ringer's solution, the following reactions would occur at anodic and cathodic regions:

At anodic regions:

$$Mg \rightarrow Mg^{+} + e^{-} \quad (1)$$

$$Mg + 2H_2O \rightarrow Mg^{2+} + 2OH^{-} + H_2 \quad (2)$$

Mg^{+} is a metastable ion. The formation of Mg^{+} ion, which is consistent with one-electron transfer kinetics and low activation energy of the corrosion process, has also been reported by Badawy et al. [69]. The occurrence of low frequency inductance loop in the Nyquist plots of CP-Mg and ZM21 Mg alloy is attributed to the existence of Mg^{+} ion. The Mg^{+} ion is easily oxidized to Mg^{2+}, which is accompanied with hydrogen evolution.

At cathodic regions:

$$2H_2O + 2e^{-} \rightarrow H_2 + 2OH^{-} \quad (3)$$

Overall reaction:

$$Mg + 2H_2O \rightarrow Mg(OH)_2 + H_2 \uparrow \quad (4)$$

The presence of higher concentrations of chloride ions in Ringer's solution will transform the insoluble $Mg(OH)_2$ into soluble $MgCl_2$ [70], resulting in the generation of excess OH^{-} and an increase in interfacial pH > 10 [71]

$$Mg(OH)_2 + 2Cl^{-} \rightarrow MgCl_2 + 2OH^{-} \quad (5)$$

Since the electrolyte solution contains Ca^{2+}, Mg^{2+} (from CP-Mg/ZM21 Mg alloy) and CO_3^{2-} ions, increase in interfacial pH > 10 would promote nucleation of $CaCO_3$ on the surface of CP-Mg and ZM21 Mg alloy. The growth of these carbonates depends on subsequent dissolution of Mg from the metal/alloy though the pores/defects of the corrosion product and the corresponding increase in interfacial pH. The morphological features, EDX analysis and FT-IR spectra suggest that the corrosion product layer is the aragonitic form of $CaCO_3$ on both CP-Mg as well as on ZM21 Mg alloy. The lateral growth and formation of a thin continuous aragonitic $CaCO_3$ film occurs on the surface of both CP-Mg as well as ZM21 Mg alloy as a first stage of growth. However, thickening of the $CaCO_3$ layer that occurs in the second stage enables an improvement in the corrosion resistance of ZM21 Mg alloy whereas this stage of growth is delayed for CP-Mg.

The change in shape of the Nyquist plots, type of corrosion products formed and the microstructural features exhibit a good correlation. A similar trend in the Nyquist plots of CP-Mg and ZM21 Mg alloy observed up to 12 and 16 h, respectively, is due to the formation of insoluble corrosion products on their surface, which hinders the charge transfer process and is reflected by the increase in R_{ct} values. The change in shape of the Nyquist plots observed between 12 and 60 h for CP-Mg and between 16 and 68 h for ZM21 Mg alloy can be correlated to the simultaneous dissolution of CP-Mg/ZM21 Mg alloy through the pores or defects and formation of the corrosion product layer following the increase in interfacial pH. The similarity in shape of the Nyquist plots observed between 60 and 92 h of CP-Mg can be correlated to a complete coverage of the surface with corrosion products having mud-crack patterns and large number of clusters of needle-like crystals (Fig. 6a), supported by a near saturation in R_{ct} and CPE_1 values. The continuous increase in the diameter of the semicircles of the Nyquist plots of ZM21 Mg alloy observed between 68 and 92 h reveals not only a complete coverage of the surface but also thickening of the corrosion product layer. The absence of mud-crack pattern on the surface of ZM21 Mg alloy is due to the complete coverage of its surface with a compact layer of well-developed rod-like crystals (Fig. 6b), which is reflected by the sudden increase in R_{ct} and decrease in CPE_1 values. Although the aragonitic form of $CaCO_3$ is formed on both CP-Mg as well as on ZM21 Mg alloy, the first stage involves a lateral growth and formation of a thin continuous aragonitic $CaCO_3$ film on the surface of CP-Mg/ZM21 Mg alloy. The second stage of growth involves thickening of the $CaCO_3$ layer that enables an improvement in the corrosion resistance. This stage of growth occurs quickly for ZM21 Mg alloy whereas it is delayed for CP-Mg.

Besides corrosion protective ability, mechanical properties such as, specific density and Young's modulus are important in terms of fabrication of implants. In this perspective, the specific density and Young's modulus of CP-Mg and ZM21 Mg alloy are closer to bone than the commonly used metallic implant materials and synthetic

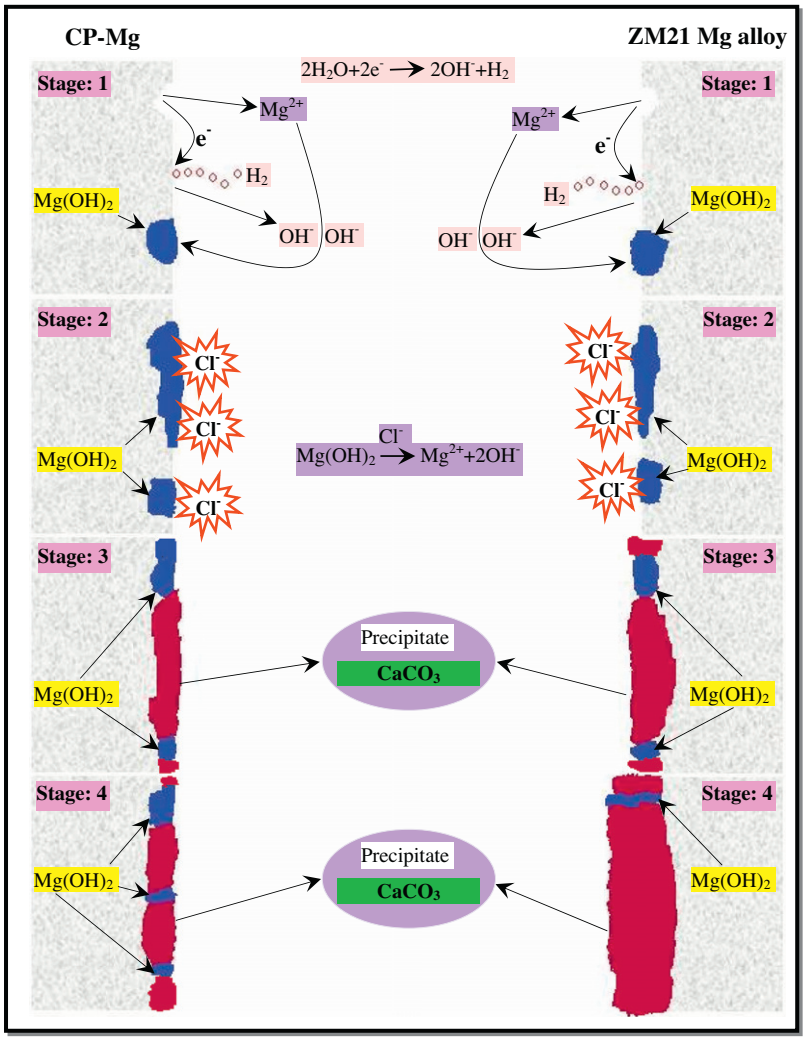

Fig. 10. Schematic explaining the various stages of the mechanism of corrosion of CP-Mg and ZM21 Mg alloy in Ringer's solution for 92 h.

Table 1
Comparison of mechanical properties of CP-Mg, ZM21 Mg alloy, other commonly used metallic implant materials and synthetic hydroxyapatite.

Mechanical property	Human bone	CP-Mg	ZM21	Ti alloys, Co–Cr alloys stainless steels	Synthetic hydroxyapatite
Specific density (g/cm^3)	1.8–2.1	1.74–2	1.78	>4	>3
Young's modulus (GPa)	3–20	41–45	43.4	>110	>70

hydroxyapatite (Table 1), which would enable a decrease in stress at the bone/implant interface, stimulate bone growth and increase the implant stability [13]. The higher fracture toughness over ceramic biomaterials, higher strength than biodegradable plastics, and favorable elastic modulus than commonly used metallic implant materials, makes Mg and its alloys as ideal choice for implant applications.

4. Conclusions

The corrosion behavior of commercially pure magnesium (CP-Mg) and ZM21 Mg alloy in Ringer's solution was evaluated by EIS during every 4 h interval for 92 h, to estimate the longevity of these materials for implant application. The terminology of "long term" though used in general for studies performed for a longer period, in years, this term is used in the present study to distinguish it from the regular electrochemical corrosion studies that are performed within an hour or two. The EIS spectra of CP-Mg and ZM21 Mg alloy shows a capacitive loop in the high frequency region, a capacitive loop in the medium frequency region and an inductive loop in the low frequency region, suggesting the involvement of three time constants. The change in R_{ct} and CPE_1 measured as a function of immersion time reveals that ZM21 Mg alloy offers a higher corrosion resistance than CP-Mg. The morphological features of CP-Mg after immersion in Ringer's solution for 92 h reveal the formation of mud-crack patterns and large number of clusters of needle-like crystals. In contrast, no mud-crack pattern was observed on the surface of ZM21 Mg alloy, which is covered with a compact layer of well-developed rod-like crystals. The EDX analysis indicates that the corrosion products formed on the surface of CP-Mg and ZM21 Mg alloy are rich in O, C, Ca and Mg and they could be a mixture of $CaCO_3$ and $Mg(OH)_2$, with $CaCO_3$ as the predominant species. The FT-IR spectra confirms that the corrosion product is a mixture of $Mg(OH)_2$ and the aragonite form of $CaCO_3$. The lateral growth and formation of a thin continuous aragonitic $CaCO_3$ film occurs on the surface of both CP-Mg as well

as ZM21 Mg alloy as a first stage of growth. However, thickening of the $CaCO_3$ layer that occurs in the second stage enables an improvement in the corrosion resistance of ZM21 Mg alloy whereas this stage of growth is delayed for CP-Mg. The change in shape of the Nyquist plots, type of corrosion products formed and the microstructural features exhibit a good correlation. The study concludes that EIS can be used as an effective tool to monitor the long-term corrosion behavior of CP-Mg and ZM21 Mg alloy in Ringer's solution. The higher corrosion protective ability of ZM21 Mg alloy in Ringer's solution compared to CP-Mg is encouraging. The results of this study suggest that ZM21 Mg alloy can be considered as a promising candidate material for the development of degradable implants.

Acknowledgement

The authors express their sincere thanks to Dr. S. Srikanth, Director, National Metallurgical Laboratory, Jamshedpur, for his keen interest and permission to publish this paper.

References

[1] F. Witte, N. Hort, C. Vogt, S. Cohen, K.U. Kainer, R. Willumeit, F. Feyerabend, Curr. Opin. Solid State Mater. Sci. 12 (2008) 63–72.
[2] G. Song, S. Song, Adv. Eng. Mater. 9 (2007) 298–302.
[3] R. Zeng, W. Dietzel, F. Witte, N. Hort, C. Blawert, Adv. Eng. Mater. 10 (2008) 155–169.
[4] B.A. Shaw, E. Sikora, S. Virtanen, Electrochem. Soc. Interface Summer (2008) 45–49.
[5] H. Tamai, K. Igaki, E. Kyo, K. Kosuga, A. Kawashima, S. Matsui, H. Komori, T. Tsuji, S. Motohara, H. Uehata, Circulation 102 (2000) 399–404.
[6] G. Mani, M.D. Feldman, D. Patel, C.M. Agrawal, Biomaterials 28 (2007) 1689–1710.
[7] M.P. Staiger, A.M. Pietak, J. Huadmai, G. Dias, Biomaterials 27 (2006) 1728–1734.
[8] B. Heublein, R. Rohde, V. Kaese, M. Niemeyer, W. Hartung, A. Haverich, Heart 89 (2003) 651–656.
[9] M. Peuster, P. Beerbaum, F.W. Bach, H. Hauser, Cardiol. Young 16 (2006) 107–116.
[10] P. Zartner, M. Buettner, H. Singer, M. Sigler, Catheter. Cardiovasc. Interv. 69 (2007) 443–446.
[11] P. Erne, M. Schier, T.J. Resink, Cardiovasc. Intervent. Radiol. 29 (2006) 11–16.
[12] H. Zreiqat, C.R. Howlett, A. Zannettino, P. Evans, G. Schulze-Tanzil, C. Knabe, M. Shakibaei, J. Biomed. Mater. Res. 62 (2002) 175–184.
[13] J. Nagels, M. Stokdijk, P.M. Rozing, J. Shoulder Elbow Surg. 12 (2003) 35–39.
[14] H.P. Wiesmann, T. Tkotz, U. Joos, K. Zierold, U. Stratmann, T. Szuwart, U. Plate, H.J. Hoehling, J. Bone Miner. Res. 12 (1997) 380–383.
[15] A. Hartwig, Mutat. Res-Fund. Mol. M 475 (2001) 113–121.
[16] J.J. Vitale, Lancet 340 (1992) 1224–1225.
[17] J. Amighi, S. Sabeti, O. Schlager, W. Mlekusch, M. Exner, W. Lalouschek, R. Ahmadi, E. Minar, M. Schillinger, Stroke 35 (2004) 22–27.
[18] A.M. Lindenberg, H. Windhugen, F. Witte, United States Patent Application 2004/0241036 A1, December 2, 2004.
[19] G. Song, Corros. Sci. 49 (2007) 1696–1701.
[20] C. Blawert, D. Fechner, D. Höche, V. Heitmann, W. Dietzel, K.U. Kainer, P. Živanović, C. Scharf, A. Ditze, J. Gröbner, R. Schmid-Fetzer, Corros. Sci. 52 (2010) 2452–2468.
[21] V. Lisitsyn, G. Ben-Hamu, D. Eliezer, K.S. Shin, Corros. Sci. 52 (2010) 2280–2290.
[22] N.T. Kirkland, J. Lespagnol, N. Birbilis, M.P. Staiger, Corros. Sci. 52 (2010) 287–291.
[23] Wei Zhou, Tian Shen, Naing Naing Aung, Corros. Sci. 52 (2010) 1035–1041.
[24] Wenjuan Liu, Fahe Cao, Bingli Jia, Liyun Zheng, Jianqing Zhang, Chunan Cao, Xiaogang Li, Corros. Sci. 52 (2010) 639–650.
[25] Wenjuan Liu, Fahe Cao, Anna Chen, Linrong Chang, Jianqing Zhang, Chunan Cao, Corros. Sci. 52 (2010) 627–638.
[26] Martin Jönsson, Dan Persson, Corros. Sci. 52 (2010) 1077–1085.
[27] Li-jing Yang, Yan-fang Li, Ying-hui Wei, Li-feng Hou, Yong-gang Li, Yun Tian, Corros. Sci. 52 (2010) 2188–2196.
[28] S.S.A. El-Rahman, Pharmacol. Res. 47 (2003) 189–194.
[29] N. Yumiko, T. Yukari, T. Yasuhide, S. Tadashi, I. Yoshio, Fund. Appl. Toxicol. 37 (1997) 106–116.
[30] W. Yang, P. Zhang, J. Liu, Y. Xue, J. Rare Earth 24 (2006) 369–373.
[31] W.C. Kim, J.G. Kim, J.Y. Lee, H.K. Seok, Mater. Lett. 62 (2008) 4146–4148.
[32] C.J. Boehlert, K. Knittel, Mater. Sci. Eng., A 417 (2006) 315–321.
[33] S.A. Khan, Y. Miyashita, Y. Mutoh, Z.B. Sajuri, Mater. Sci. Eng., A 420 (2006) 315–321.
[34] B.E. Carlson, J.W. Jones, The metallurgical aspects of the corrosion behavior of cast Mg–Al alloys, in: Light Metals Processing and Applications, METSOC Conference, Quebec, 1993.
[35] I.J. Polmer, Physical Metallurgy of Magnesium Alloys, DGM Informationsgesellschaft, Oberursel, Germany, 1992. p. 201.
[36] L. Xu, G. Yu, E. Zhang, F. Pan, K. Yang, J. Biomed. Mater. Res. A 83 (2007) 703–711.
[37] E. Zhang, D. Yin, L. Xu, L. Yang, K. Yang, Mater. Sci. Eng., C 29 (2009) 987–993.
[38] Y. He, H. Tao, Y. Zhang, Y. Jiang, S. Zhang, C. Zhao, J. Li, B. Zhang, Y. Song, X. Zhang, Chinese Sci. Bull. 54 (2009) 484–491.
[39] F. Rosalbino, S. De Negri, A. Saccone, E. Angelini, S. Delfino, J. Mater. Sci.: Mater. Med. 21 (2010) 1091–1098.
[40] M. Azzi, J.A. Szpunar, Biomol. Eng. 24 (2007) 443–446.
[41] M. Azzi, M. Paquette, J.A. Szpunar, J.E. Klemberg-Sapieha, L. Martinu, Wear 267 (2009) 860–866.
[42] Satendra Kumar, T.S.N. Sankara Narayanan, J. Alloy. Compd. 479 (2009) 699–703.
[43] Satendra Kumar, T.S.N. Sankara Narayanan, S. Ganesh Sundara Raman, S.K. Seshadri, Mater. Sci. Eng., C 29 (2009) 1942–1949.
[44] Satendra Kumar, T.S.N. Sankara Narayanan, S. Ganesh Sundara Raman, S.K. Seshadri, Mater. Chem. Phys. 119 (2010) 337–346.
[45] Satendra Kumar, T.S.N. Sankara Narayanan, S. Ganesh Sundara Raman, S.K. Seshadri, Corros. Sci. 52 (2010) 711–721.
[46] Satendra Kumar, T.S.N. Sankara Narayanan, S. Ganesh Sundara Raman, S.K. Seshadri, Tribol. Int. 43 (2010) 1245–1252.
[47] Satendra Kumar, B. Sivakumar, T.S.N. Sankara Narayanan, S. Ganesh Sundara Raman, S.K. Seshadri, Wear 268 (2010) 1537–1541.
[48] J.R. Morlidge, P. Skeldon, G.E. Thompson, H. Habazaki, K. Shimizu, G.C. Wood, Electrochim. Acta 44 (1999) 2423–2435.
[49] G. Baril, C. Blanc, N. Pebere, J. Electrochem. Soc. 148 (2001) B489–496.
[50] Y. Zhang, C. Yan, F. Wang, W. Li, Corros. Sci. 47 (2005) 2816–2831.
[51] Y.C. Xin, C.L. Liu, W.J. Zhang, K. Huo, G. Tang, X. Tian, P.K. Chu, J. Mater. Res. 23 (2008) 312–317.
[52] Y.C. Xin, C.L. Liu, K. Huo, G. Tang, X. Tian, P.K. Chu, Surf. Coat. Technol. 203 (2009) 2554–2557.
[53] Y. Song, D. Shan, R. Chen, F. Zhang, E.H. Han, Mater. Sci. Eng., C 29 (2009) 1039–1045.
[54] W.A. Anderson, H.C. Stumpf, Corrosion 36 (1980) 212–220.
[55] O. Lunder, T.K.R. Akune, K. Nisancioglu, Corrosion 43 (1987) 291–295.
[56] J. Schlomach, K. Quarch, M. Kind, Chem. Eng. Technol. 29 (2006) 215–220.
[57] F.C. Meldrum, S.T. Hyde, J. Cryst. Growth 231 (2001) 544–558.
[58] A. Katz, Geochim. Cosmochim. Acta 37 (1973) 1563–1586.
[59] O. Sohnel, J.W. Mullin, J. Cryst. Growth 60 (1982) 239–250.
[60] A. Mucci, J.W. Morse, Geochim. Cosmochim. Acta 47 (1983) 217–233.
[61] T.G. Sabbides, P.G. Koutsoukos, J. Cryst. Growth 133 (1993) 13–22.
[62] C.Y. Tai, F.B. Chen, AIChE J. 44 (1998) 1790–1798.
[63] M.M. Reddy, K.K. Wang, J. Cryst. Growth 50 (1980) 470–480.
[64] M.M. Reddy, G.H. Nancollas, J. Cryst. Growth 35 (1976) 33–38.
[65] H.B. Yao, Y. Li, A.T.S. Wee, Appl. Surf. Sci. 158 (2000) 112–119.
[66] L. Wang, B.P. Zhang, T. Shinohara, Mater. Des. 31 (2010) 857–863.
[67] H.P. Godard, W.B. Lepson, M.R. Bothewell, R.L. Kane, The Corrosion of Light Metals, New York, Willey, 1967.
[68] J.Y. Uan, B.L. Yu, X.L. Pan, Metall. Mater. Trans. A 39A (2008) 3233–3245.
[69] W.A. Badawy, N.H. Hilal, M.E. Rabiee, H. Nady, Electrochim. Acta 55 (2010) 1880–1887.
[70] Z. Li, X. Gu, S. Lou, Y. Zheng, Biomaterials 29 (2008) 1329–1344.
[71] A. Simaranov, I. Sokolova, A. Marshakov, Y. Mikhailovskii, Prot. Metal 27 (1991) 329–334.